PNAS RESEARCH ARTICLE | BIOPHYSICS AND COMPUTATIONAL BIOLOGY OPEN ACCESS

Conserved and divergent chaperoning effects of Hsp60/10 chaperonins on protein folding landscapes

Anwar Sadat[a,b,1], Satyam Tiwari[b,1], S. Sunidhi[c,2], Aseem Chaphalkar[a,b,2], Manisha Kochar[a,b], Mudassar Ali[d], Zainab Zaidi[a,b], Akanksha Sharma[a,b], Kanika Verma[a,b], Kannan Boosi Narayana Rao[a,b], Manjul Tripathi[b], Asmita Ghosh[a,b], Deepika Gautam[a,b], Atul[c], Arjun Ray[c,3], Koyeli Mapa[a,d,3,4], and Kausik Chakraborty[a,b,3]

Edited by Ulrich Hartl, Max Planck Institute of Chemistry, Martinsried, Germany; received October 25, 2021; accepted March 2, 2022

The GroEL/ES chaperonin cavity surface charge properties, especially the negative charges, play an important role in its capacity to assist intracavity protein folding. Remarkably, the larger fraction of GroEL/ES negative charges are not conserved among different bacterial species, resulting in a large variation in negative-charge density in the GroEL/ES cavity across prokaryotes. Intriguingly, eukaryotic GroEL/ES homologs have the lowest negative-charge density in the chaperonin cavity. This prompted us to investigate if GroEL's chaperoning mechanism changed during evolution. Using a model in vivo GroEL/ES substrate, we show that the ability of GroEL/ES to buffer entropic traps in the folding pathway of its substrate was partially dependent upon the negative-charge density inside its cavity. While this activity of GroEL/ES was found to be essential for *Escherichia coli*, it has been perfected in some organisms and diminished in others. However, irrespective of their charges, all the tested homologs retained their ability to regulate polypeptide chain collapse and remove enthalpic traps from folding pathways. The ability of these GroEL/ES homologs to buffer mutational variations in a model substrate correlated with their negative-charge density. Thus, Hsp60/10 chaperonins in different organisms may have changed to accommodate a different spectrum of mutations on their substrates.

protein folding | chaperone | mutational buffering

A multimeric, barrel-shaped complex of Hsp60 and Hsp10 proteins forms an essential chaperone (also known as chaperonin) system in most life forms (1). Representative members of this system are found in all prokaryotes—barring some tenericutes—and in the compartments of endosymbiotic origin in all eukaryotes. *Escherichia coli* Hsp60/Hsp10, also known as GroEL/GroES (referred to as GroEL/ES), is the best-studied member of the Hsp60/Hsp10 (referred to as Hsp60/10) family. Extensive studies on GroEL/ES as a canonical Hsp60/10 chaperone have revealed important mechanistic insights on the molecular mechanism of folding assistance by this group of chaperones but whether the chaperoning mechanisms of GroEL/ES persisted over evolution is still elusive (1, 2).

Despite significant controversies regarding GroEL/ES's chaperoning mechanism, it is well established that at least a subset of its substrates is assisted for its folding by encapsulation within the chaperonin cavity. Thus, the cavity charge property of the GroEL/ES and Hsp60/10s would be immensely important in determining their chaperoning mechanism. To address this, we computationally compared the GroEL/ES's cavity charge property with several of its eubacterial, hyperthermophilic bacterial and some eukaryotic homologs. Interestingly, we found significant variation in cavity charge among the different Hsp60/10 homologs. While the net negative charge of the chaperonin cavity was mostly conserved in eubacterial GroEL/ES homologs, hyperthermophilic and eukaryotic homologs contain drastically decreased negatively charged cavities. To understand the changes in the chaperoning mechanism with altered cavity charges, we employed laboratory-evolved and endogenous in vivo substrates of GroEL/ES to compare the folding assistance offered by GroEL/ES and its representative homologs.

We have shown that the negatively charged cavity wall of the GroEL/ES system acts like a high-density array of chemical chaperones to edit the protein-folding landscape. It reroutes folding to deviate from the path determined by the amino acid sequence of the substrate and take a route with a lower entropic barrier. Remarkably, the density of negative charges inside the cavity determined the capacity of this chaperonin to assist folding and buffer mutational variations of a model substrate in vivo. Since the density of this charge showed a large variation across different species, we posit that the evolvability of the chaperonin substrates varies between different organisms based on the

Significance

Hsp60/10 chaperonins are critical for cellular proteostasis in all kingdoms of life. In this study, we present that Hsp60/10 across different species have differences in the cavity properties and correlatively in their capability to remove entropic traps in folding pathways of GroEL/ES substrates; this is affected majorly by differences in the negative-charge density inside the chaperonin cavity. This dissimilarity leads to a remarkable difference between Hsp60/10 homologs in buffering mutational variations. However, most of them can remove nonnative contacts during folding of their substrates and alter the way the polypeptide chain undergoes hydrophobic collapse. We show that these homologs may have evolved specific modes of folding assistance by modulating cavity properties according to the requirements of their substrates.

Author contributions: K.C. and K.M. designed research; A. Sadat, S.T., A.C., M.K., M.A., Z.Z., K.V., K.B.N.R., M.T., A.G., D.G., and K.C. performed research; A. Sadat, S.T., S.S., K.V., A.G., A.R., K.M., and K.C. contributed new reagents/analytic tools; S.S., A. Sharma, Atul, A.R., K.M., and K.C. analyzed data; and A.R., K.M., and K.C. wrote the paper.

The authors declare no competing interest.

This article is a PNAS Direct Submission.

[1]A. Sadat and S.T. contributed equally to this work.

[2]S.S. and A.C. contributed equally to this work.

[3]A.R., K.M., and K.C. contributed equally to this work.

[4]To whom correspondence may be addressed. Email: koyeli.mapa@snu.edu.in.

This article contains supporting information online at http://www.pnas.org/lookup/suppl/doi:10.1073/pnas.2118465119/-/DCSupplemental.

Published April 29, 2022.

cavity properties of the chaperonin. Interestingly, GroEL/ES also possesses a contrasting function of preventing nonnative contacts in its substrates. This function is shared between all the bacterial and eukaryotic Hsp60/10 chaperones tested. Thus, we show that this chaperonin system has the following two central mechanisms to assist folding: 1) a conserved mechanism to prevent the formation of nonnative contacts, and 2) a variable mechanism to aid folding with its negatively charged cavity by lowering entropic barriers.

Results and Discussion

Negative Charge Density in Cavity Varies between GroEL/ES Homologs. Small molecules containing zwitterionic moieties, multiple hydroxyl groups, or charged groups are known to act as chemical chaperones (3). They can accelerate refolding rates of proteins in vitro (4) and help proteins to fold in vivo (5, 6). Since GroEL/ES assists in folding of a subset of its substrates after encapsulation within its cavity (7), we asked if these groups are abundant in GroEL/ES's cavity. We identified the inner-lining residues using the Characterization of Inner Cavity Lining of Proteins (CICLOP) tool (8) and found 208 negatively charged, 123 positively charged, and 72 hydroxyl groups facing the inner cavity (Fig. 1*A*). Given that the volume of *cis*-cavity is ∼175,000 Å^3, approximate effective concentrations of the respective groups inside the *cis*-cavity are 2M, 1.2M, and 0.7M, respectively. At these concentrations, small molecules having these groups can effectively accelerate protein folding in vitro (4).

To understand the importance of these lining residues in accelerating protein folding inside the Hsp60/10 chaperonin cavities in general, we measured the conservation of these active groups during evolution. We modeled GroEL/ES homologs from 87 different bacterial strains. Additionally, we modeled homologs from 27 hyperthermophilic bacteria and 6 eukaryotes as representatives of species that have different proteostasis requirements; while thermophiles need to fold proteins at a higher temperature, eukaryotic mitochondrial Hsp60/10 would have to deal with a more complex eukaryotic proteome and higher temperature in mitochondria (9). All organisms that we chose for the cavity inner surface charge analysis possess 1) one GroEL homolog with >50% identity to facilitate high-confidence modeling and 2) a single GroEL/ES homolog to restrict our analysis to the homologs that are dedicated to protein folding (10). We modeled all the homologs (minimum sequence identity = 50.5%, minimum coverage = 94.5%; *SI Appendix*, Table S1) based on Protein Data Bank (PDB) 1AON, validated the models using template modeling (TM) score (minimum TM score, >0.68) (11) (*SI Appendix*, Table S1), and identified the cavity lining residues using CICLOP (8). The number of hydroxyl groups (Fig. 1 *B*, *Top*) was variable among the bacterial homologs (coefficient of variation [CV] = 15.3%), while the number of positively charged groups (Fig. 1 *B*, *Middle*) exhibited lower variability (CV = 6.9%). The number of negatively charged groups (Fig. 1 *B*, *Bottom*) showed the least variability between bacterial homologs (CV = 4.3%) among the three types of residues tested, indicating that the number of negatively charged residues are more conserved in bacterial species.

We focused on the *cis*-cavity–mediated folding for this work. *Cis*-cavity is formed when GroEL binds to GroES in the presence of adenosine triphosphate (ATP) to form an asymmetric bullet-shaped structure. GroES caps one end of the tetradecameric GroEL cage, forming the *cis*-cavity, while the other end of GroEL, free of GroES, remains as an open cavity denoted as the *trans*-cavity. Since many of the well-characterized substrates of *E. coli* GroEL/ES (eco EL/ES) are found inside the *cis*-cavity, active groups that assist folding of proteins encapsulated within the chaperonin cavity should be more abundant in the *cis*-cavity. Comparing the abundance of all the 20 amino acids (*SI Appendix*, Fig. S1*A*), we found that only Arg, Glu, Asp, and Lys show statistically significant enrichment inside the *cis*-cavity over the *trans*-cavity. After we grouped the amino acids with similar charges, negatively charged groups were ∼1.6-fold higher, while the positively charged residues were only ∼1.2-fold higher in the *cis*-cavity than in the *trans*-cavity in bacterial homologs (Fig. 1*C*). The number of hydroxyl groups did not change significantly between the *cis*- and *trans*-cavity (Fig. 1*C*). This indicates that the negatively and positively charged groups may play an important role in the function of bacterial GroEL/ES homologs. This is consistent with findings that conserved negative charges are important contributors to chaperonin-assisted folding (12, 13). Interestingly, the eukaryotic homologs show a marked decrease in negative charges in the *cis*-cavity (Fig. 1 *B*, *Top*), indicating a possible divergence in the chaperoning mechanism.

Since the electrostatic potential inside the cavity depends on the distribution of negative and positive charges on surface lining the cavity, we devised a protocol for calculating the charge potential at the center of the *cis*- and *trans*-cavity of GroEL/ES and its homologs from their structure. This calculates effective electrostatic potential based on the total charge distribution on GroEL (that varies between organisms) and that of GroES (that does not show any correlated changes between organisms). The *cis*-cavity shows an 18% higher effective negative charge than the *trans*-cavity and is conserved across different homologs (13% higher effective negative charge in the *cis*-cavity, P = 1.3E-18). Interestingly, the effective negative charge inside the cavity (both *cis* and *trans*) showed a large variance between species (Fig. 1*D*). Hyperthermophilic bacteria and eukaryotes showed a significantly lower effective negative charge in the cavity than nonhyperthermophilic bacteria (Fig. 1*D*). Although we have used an asymmetric GroEL/ES structure to model the human Hsp60/10 (hHsp60/10) homolog, the crystal structure available for hHsp60/10 is in the symmetric state with two back-to-back *cis*-cavities. We checked if the surface charge distribution of the *cis*-cavity from the modeled asymmetric structure was consistent with the charge distribution in the symmetric cavities formed in the crystal structure. Indeed, the cavity surface of a symmetrical hHsp60/10, whose crystal structure is known (14), had a lower negative charge than the *cis*-cavity of the GroEL/ES system (Fig. 1*E*). Similar observations were made on a modeled asymmetric complex of hHsp60/10 or yeast Hsp60/10 (yHsp60/10) complex (Fig. 1*E*). This indicated that a negatively charged cavity surface may not be conserved in eukaryotic Hsp60/10 homologs. As negative charges of eco EL/ES have been shown to play an important role in helping proteins fold inside the cavity (12), variation in the charge density among GroEL/ES homologs suggests that the ability of these chaperonins to affect negative-charge-assisted folding may not have been conserved during evolution. This also provides us with a handle to determine the role of nonconserved negative charges in GroEL/ES-assisted folding.

Negative Charge Density Contributes toward Chaperoning Capacity. To see if the effective charge density in the *cis*-cavity is important for GroEL/ES activity in vivo, we chose a bacterial homolog that is more (*Cellulomonas flavigena*; hereafter referred

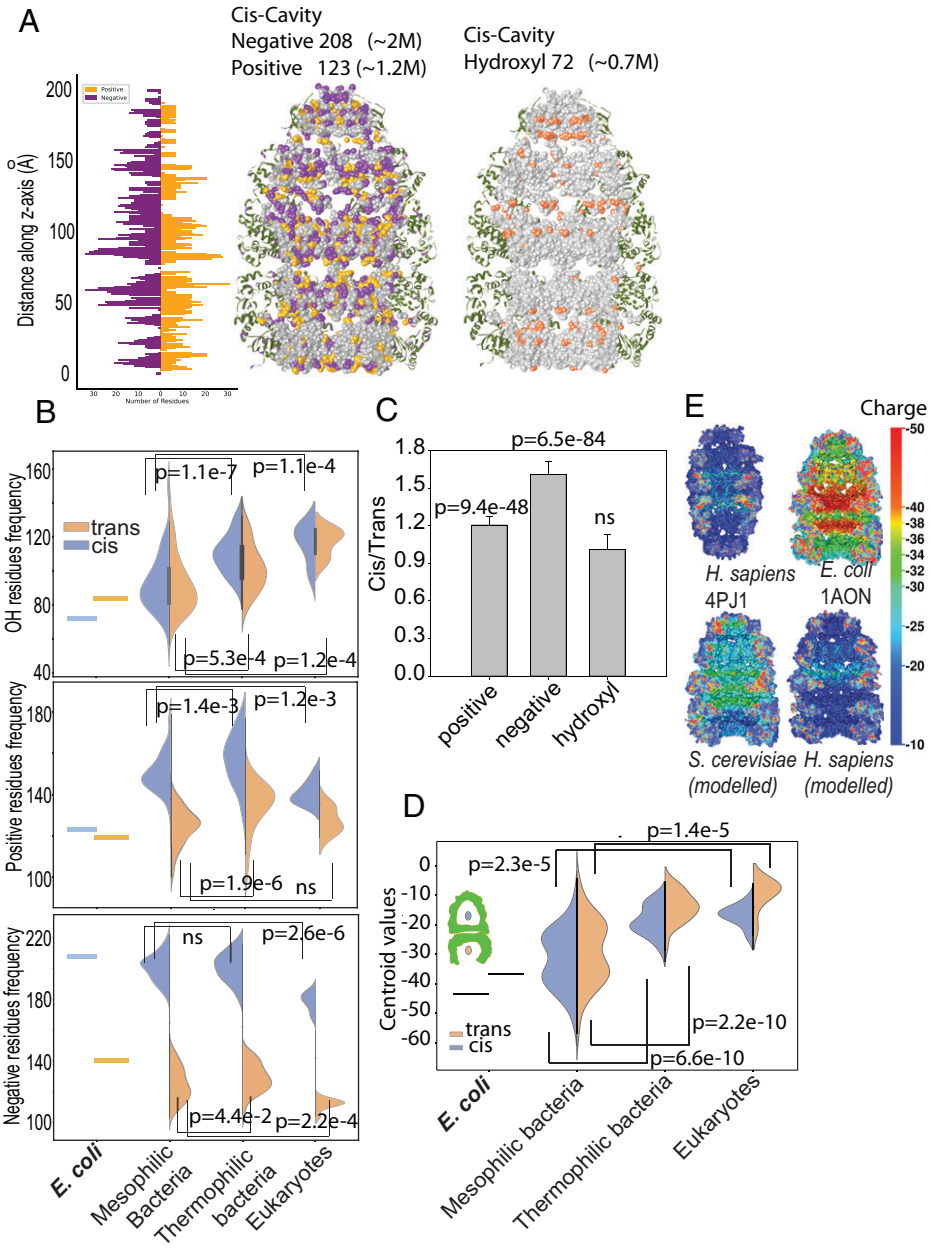

Fig. 1. The charge density of Hsp60/10 homologs varies between organisms. (*A*) The inner physicochemistry of the core cavity of GroEL/ES. Using CICLOP (8), the inner residues, represented as spheres, are mapped onto the structure (*Right*) with different chemical residues colored according to the mentioned properties. The properties, as a function of the *z* axis, are also mapped to elucidate the underlying distribution of the chemical residues. (*B*) Comparison of the frequency of hydroxyl groups, positive amino acid residues, and negative amino acid residues lining the inner cavity of GroEL (from *Top* to *Bottom*, respectively). The comparisons are both intracategorical (*cis* and *trans* of the same group) and intercategorical (between *E. coli*, bacteria, hyperthermophilic bacteria, and eukaryotes). Mann–Whitney *U* test was used to calculate the significance of the intercategorical difference in frequencies, by taking the bacteria group as the reference. The corresponding *P* values are mentioned. (*C*) The ratio of positively charged groups, negatively charged groups, or hydroxyl groups lining the *cis*-cavity to their numbers in the *trans*-cavity of bacterial homologs is shown along with the *P* values for the difference between the *cis*- and *trans*-cavity. A paired, two-tailed Student's *t* test was applied. ns, not significant. (*D*) Centroid value comparison between bacteria, thermophilic bacteria, and eukaryotes. Mann–Whitney *U* test is used to establish the significance in differences by taking bacteria as the reference group, and *P* values (Mann–Whitney two-tailed) are reported. (*E*) Charge distribution in the symmetric complex of hHsp60/10 (PDB: 4PJ1), eco EL/ES, and modeled structures of yHsp60/10 and hHsp60/10. The electrostatics of the molecules are mapped to the molecular surface of the chaperonins. Electrostatic potentials were calculated using adaptive Poisson–Boltzmann solver (ABPS) (35), and the representation was made using Chimera. The color scale, ranging from −50 to −10, shows the most negative regions as red and the least negative one as blue.

to as cfl) and one that is less (*Candidatus* Sulcia muelleri; hereafter referred to as smh) negatively charged than eco EL/ES (Fig. 2*A*). Additionally, we took hHsp60/10 and *Saccharomyces cerevisiae* Hsp60/10 (yHsp60/10) as representatives of eukaryotic homologs with a less negatively charged cavity than eco EL/ES (Fig. 2*A*). To check if the cavity surface charges would contribute to the difference between GroEL/ES and Hsp60/10 systems, we generated chimera of GroEL-Hsp60 complexes where negatively charged regions of the GroEL/ES system (Fig. 2*B*) were replaced with the homologous regions from Hsp60 of yeast (y-EL) or human (h-EL) (Fig. 2*B* and *SI Appendix*, Fig S1 *B* and *C*). Complementary chimeric constructs with the negatively charged region of GroEL grafted in either yHsp60 or hHsp60 could not be expressed, but the chimeric constructs

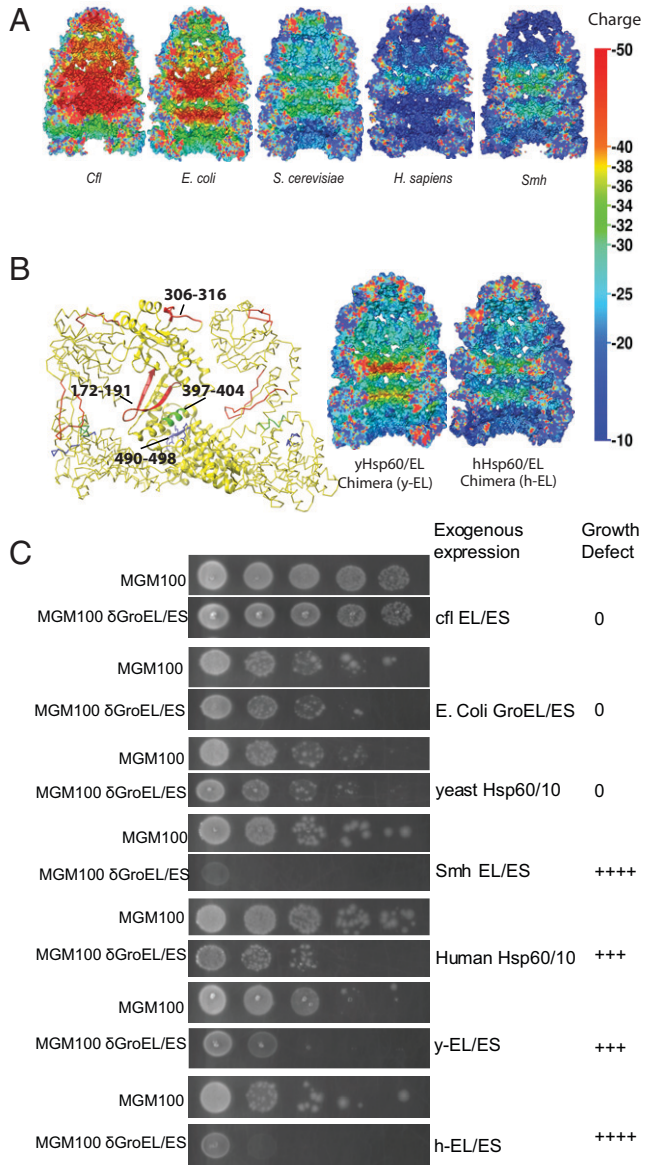

Fig. 2. Correlation between negative charge density inside chaperonin cage and their in vivo activity. (*A*) Charge distribution in modeled structures of *C. flavigena* GroEL/ES (*Left*), followed by eco EL/ES, yHsp60/10, hHsp60/10, and *Ca.* Sulcia muelleri GroEL/ES systems. The electrostatics of the molecules are mapped to the molecular surface of the chaperonins (as in Fig. 1*D*). The color scale shows the most-negative regions as red and the least-negative one as blue. (*B*) Four chains of GroEL (*cis*-cavity) are shown the exchanged regions in the chimeric constructs of GroEL/ES and Hsp60s [PDB: 1AONG (33), *cis*-cavity, GroES not drawn]. For clarity, only the central GroEL subunit is marked. Marked regions in different colors in the GroEL ring are exchanged with the homologous region from hHsp60 and yHsp60. The exchanged regions in GroEL are 172 to 191 (red), 306 to 316 (maroon), 397 to 404 (green), and 490 to 498 (blue). Homology models of chimeric constructs of yeast Hsp60 and GroEL (y-EL) (*Left*); hHsp60 and h-EL (*Right*). A cross-section of the molecule is shown along with the mapping of the electrostatic potential on the molecular surface of the protein to depict the charge distribution. The color scale is the same as shown earlier. (*C*) Spot assay of the MGM100 strain containing different overexpressing GroEL/ESs (cfl-EL/ES, eco EL/ES, yHsp60/10, smh-EL/ES, hHsp60/10, y-EL/ES, h-EL/ES). All the MGM100 strains containing overexpressing EL were grown until an optical density of 1 was reached and were serially diluted by a factor of 10. An equal volume of cultures was spotted on an LB agar plate with 0.2% glucose (panel showing GroEL depletion, labeled as MGM100-δGroEL/ES) or without glucose (panels showing MGM100 without GroEL/ES depletion, labeled as MGM100) and 100 μg ampicillin and was grown for 12 h. Growth defect is the growth difference between MGM100 and MGM100-dGroEL/ES carrying each of the exogenous Hsp60/10 homologs. 0 indicates no growth defect and number of "+" signs indicates the number of dilutions that show a growth defect. The more "+", the more growth defect. These are shown in a separate column.

y-EL and h-EL and all the other chosen GroEL/ES homologs expressed well in *E. coli* cells (*SI Appendix*, Fig. S2*A*). As primary sequences of y-EL and h-EL chimeric constructs were significantly different from GroEL/ES and were not naturally derived, we characterized them to ensure they retained structural and allosteric features of GroEL/ES. Importantly, y-EL and h-EL formed higher-order functional complexes (*SI Appendix*, Fig. S2*B*). Although a part of h-EL eluted at volumes corresponding to the single ring of GroEL, this was not an indication of inactivity, as hHsp60, the parental chaperonin from which the insertion sequences are derived, is known to form single-ring toroids (15). Moreover, most of h-EL ran as a tetradecamer in a native polyacrylamide gel electrophoresis indicating the formation of functional oligomers (*SI Appendix*, Fig. S2*C*). Furthermore, in a continuous cycling ATPase assay, GroES was able to decrease the ATPase rate of y-EL and h-EL to the same extent as observed with GroEL (*SI Appendix*, Fig. S2*D*). This decrease by GroES ensured that 1) GroES and ATP bind properly to the engineered GroELs and 2) the negative allosteric interactions between the two rings of the toroids are intact. y-EL and h-EL also were able to encapsulate the proteins inside the cavity efficiently as shown below (*SI Appendix*, Fig. S3*C*). Additionally, these were able to remove enthalpic traps as efficiently as all the other native Hsp60/10 homologs (see Fig. 4*D*), accelerate folding at 35 °C (see Fig. 4*A*), and assist identified yHsp60/10-dependent substrates in vivo (see Fig. 5*K*). All these suggest that the designed chimeric proteins retained the basic allosteric framework and interactions observed in GroEL/ES.

To see if all the chaperonin homologs have activities like eco EL/ES, we checked their ability to complement the loss of endogenous GroEL/ES. The MGM100 strain of *E. coli* harbors the endogenous copy of eco GroEL/ES under a glucose-repressible promoter (*SI Appendix*, Fig. S2*E*). Since GroEL/ES is essential for *E. coli* growth, cells cannot grow in glucose without a functional GroEL/ES expressing from a complementing plasmid (*SI Appendix*, Fig. S2*F*). Interestingly, while all the highly negatively charged GroEL/ES homologs efficiently complemented the loss of endogenous GroEL/ES in *E. coli*, the two least negatively charged homologs of GroEL/ES from human and *Ca.* Sulcia muelleri, were unable to complement the loss of GroEL/ES (Fig. 2*C* and *SI Appendix*, Fig. S2*G*). The chimeric GroEL constructs, namely, y-EL and h-EL, that had a less negatively charged cavity than GroEL partially complemented the loss of GroEL/ES. Even among these two chimeric constructs, y-EL, the more negatively charged among the two, was able to complement the loss of eco GroEL/ES better than h-EL. Thus, negative-charge density inside the chaperonin cavity partially correlated with the ability of the homologs to replace the activity of eco EL/ES in vivo. Since GroEL/ES is essential in *E. coli* as it caters to fold essential substrate proteins (7), the negative charges may be essential to fold the obligate substrates of eco EL/ES in vivo.

Cavity Negative Charges Contribute toward Entropic Assistance for GroEL/ES Substrates. To check if these chaperonins differ in their ability to assist the folding of GroEL/ES substrates in vivo, we used sGFP and MetK. sGFP is a recently described model substrate of GroEL/ES that can quantitatively report the ability of chaperonin assistance in vivo and in vitro (16), and MetK is a known endogenous substrate of GroEL/ES (7). Additionally, the folding landscape of sGFP in the presence and absence of GroEL/ES has been well characterized, providing us with a tool to understand the differences between the chaperonins in terms

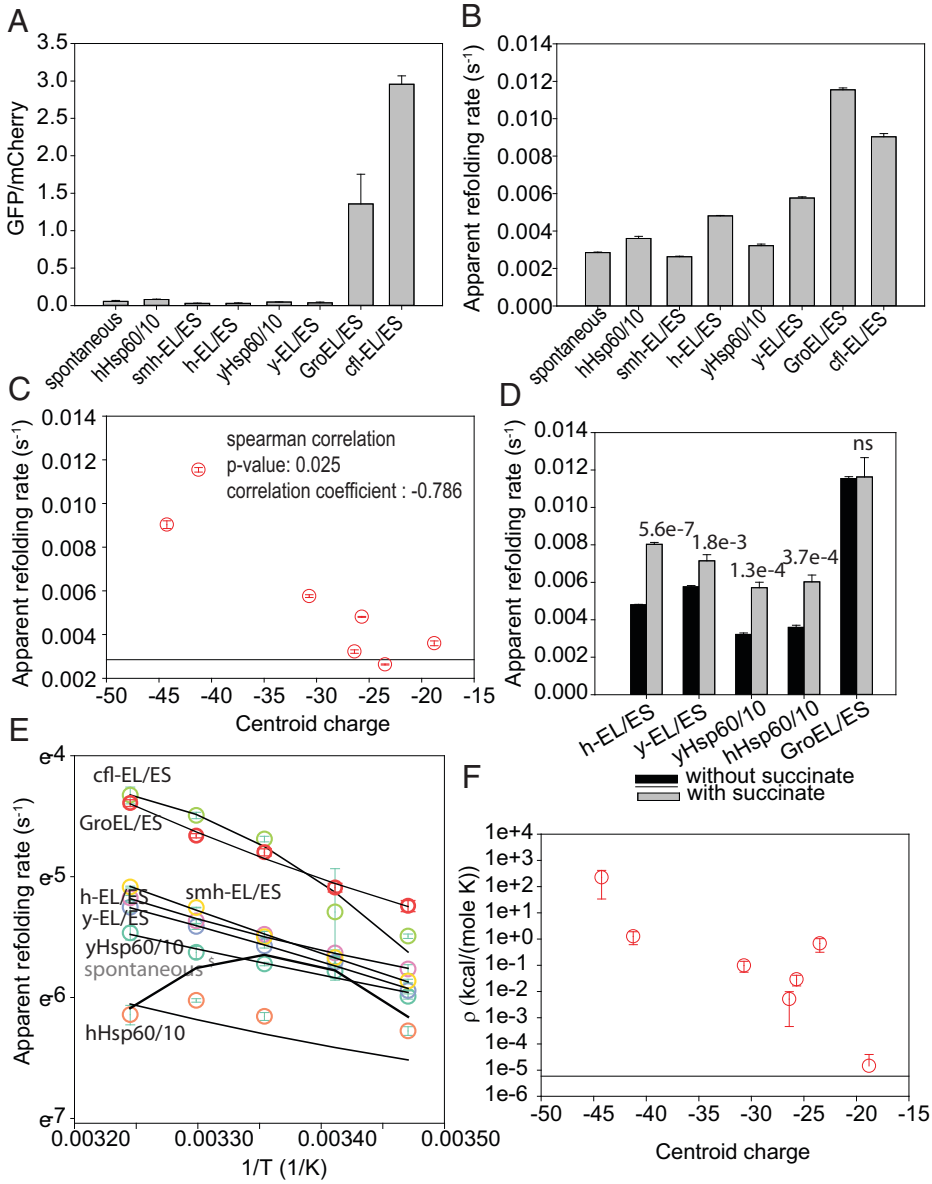

Fig. 3. Negative charges inside the cavity change the entropic component of the substrate folding landscape. (*A*) In vivo fluorescence of sGFP normalized with respect to mCherry in *E. coli* in the absence of overexpressed chaperonins or presence of overexpressing EL/ES systems from different organisms (hHsp60/10, smh-EL/ES, h-EL/ES, yHsp60/10, y-EL/ES, GroEL/ES, and cfl-EL/ES, arranged in ascending order of negative charge density in the *cis*-cavity). Error bar represents SD from three different experiments. (*B*) Apparent refolding rates of sGFP in the absence of any chaperonins or in the presence of chaperonin complexes (hHsp60/10, smh-EL/ES, h-EL/ES, yHsp60/10, y-EL/ES, GroEL/ES, and cfl-EL/ES, arranged in ascending order of negative charge density in the *cis*-cavity) and ATP in buffer A. (*C*) Correlation between the apparent rate of refolding of sGFP in the presence of different chaperonins and the centroid charge density of the chaperonins. (*D*) Apparent rate of refolding of sGFP in the presence of eco EL/ES, yHsp60/10, hHsp60/10, y-EL/ES, and h-EL/ES with (gray) and without (black) succinate (100 mM) in buffer A. (*E*) Arrhenius plot showing the dependence of the apparent rate of refolding of sGFP alone or in the presence of different chaperonin complexes at different temperatures (15 °C, 20 °C, 25 °C, 30 °C, and 35 °C). Solid lines shown fit the Eyring–Arrhenius equation. Error bars are SDs of three independent experiments. [$]Dashed bar for spontaneous folding is from published parameters (16). (*F*) The calculated ρ values obtained from Arrhenius fitting of sGFP refolding shown in *E* plotted against centroid charge density for different chaperonins.

of their ability to change the folding landscape of its substrates (16).

sGFP is a slow folding mutant of yeGFP that is rapidly degraded in vivo (16). With GroEL/ES overexpression, the protein folds efficiently and shows enhanced activity (fluorescence) in vivo. sGFP fluorescence increased with GroEL/ES expression as reported (Fig. 3*A*) (16). This increase was more prominent upon overexpression of cfl-EL/ES, the more negatively charged GroEL/ES homolog (Fig. 3*A*). The less negatively charged prokaryotic homologs or the chimeric constructs did not assist sGFP folding in vivo (Fig. 3*A*), suggesting that lowering the negative charge density in GroEL/ES cavity decreases its chaperoning capacity. The eukaryotic chaperonins were also ineffective in assisting sGFP activity in vivo (Fig. 3*A*). This corroborated well with the capability of negatively charged chaperonins to complement GroEL/ES loss in vivo. To check if this difference between the chaperonins was restricted to sGFP, we measured the solubility of an authentic endogenous substrate of GroEL/ES, MetK (7), in the presence of a subset of the chaperonins (cfl-EL/ES, smh-EL/ES, y-EL/ES, h-EL/ES, and GroEL/ES). Consistent with sGFP data, overexpressing cfl-EL/ES or GroEL/ES efficiently solubilized MetK, while solubility was lower in the presence of the other chaperonins (*SI Appendix*, Fig. S3*A*). This and the in vivo complementation data showed less negatively charged chaperonins that are naturally occurring or artificially designed are poor chaperones for GroEL/ES substrates in vivo.

To check if these chaperonin homologs were unable to enhance sGFP activity in vivo because of their inability to assist sGFP's folding, we reconstituted sGFP refolding in the presence and absence of different chaperonins in vitro. All the chaperonins (in the absence of Hsp10 and ATP) retained their ability to bind unfolded sGFP and prevented it from refolding spontaneously (*SI Appendix*, Fig. S3*B*). In the presence of ATP and its cochaperone, GroES, GroEL accelerated the refolding rate of sGFP as reported earlier (16) (Fig. 3*B*). In the presence of ATP and their respective cochaperones, cfl-EL/ES was able to accelerate the refolding of sGFP to the same extent as that of GroEL/ES. By contrast, other chaperonins were unable to accelerate the spontaneous refolding rate of sGFP further. Importantly, the chimeric constructs of GroEL/ES, harboring less negative charge regions from hHsp60 or yHsp60, did not accelerate the spontaneous refolding of sGFP under these conditions. To rule out the possibility that sGFP is not efficiently encapsulated by the different chaperonins, we took advantage of the fact that substrates, if encapsulated by ATP, can be trapped in the cavity using AlF_x that forms ADP-AlF_x and locks the complex (17). Under these conditions, anisotropy of encapsulated sGFP folded inside the cavity would be higher than the one folding in solution. All the ADP-AlF_x-trapped chaperonin complexes showed significantly higher anisotropy for sGFP than in solution (*SI Appendix*, Fig. S3*C*), demonstrating efficient encapsulation of the substrate. Thus, their difference in folding assistance was not due to their problems with substrate encapsulation. In vitro refolding rates in the presence of different chaperonins correlated positively with the activity of sGFP measured in vivo while overexpressing the chaperonins (*SI Appendix*, Fig. S3*D*). Thus, in vivo assistance by these chaperonins was dependent upon their ability to assist sGFP folding. Chaperonin-assisted folding rates showed a significant negative correlation with the charge density of the chaperonin cavity (Fig. 3*C*), suggesting a role of the negative charge density in determining their potential to assist sGFP folding. If the negative charges played a role in accelerating sGFP refolding, increasing negative charges in the hHsp60 or yHsp60 cavity would help in accelerating sGFP refolding by these chaperonins. These constructs, as discussed earlier, were designed but could not be expressed. In the absence of this construct, we increased negative charges in the cavity of less negatively charged chaperonins by adding a high concentration of a negatively charged small molecule, succinate, in the refolding buffer. If the negative charges in GroEL/ES's inner cavity surface contributed toward accelerated refolding of sGFP, the refolding rate inside the Eco-GroEL/ES cavity would not be further enhanced in the presence of a negatively charged small molecule, while this molecule should be able to help yHsp60/10 or hHsp60/10 in refolding sGFP. Indeed, 100 mM succinate increased the chaperonin-assisted refolding rate of sGFP for the less negatively charged chaperonins, while the GroEL/ES-assisted rate remained unchanged (Fig. 3*D*). Interestingly, the refolding rate of sGFP with the eukaryotic chaperonins hHsp60/10 and yHsp60/10 increased to match the GroEL/ES-assisted rate of refolding with 10 mM succinate, while it did not increase the GroEL/ES-dependent refolding rate (*SI Appendix*, Fig. S3*E*). The spontaneous refolding rate of sGFP did not increase with 10 mM succinate, and the pattern of increase in the refolding rate with increasing succinate concentration differed starkly between spontaneous refolding and hHsp60/10- or yHp60/10-dependent refolding. This indicated that additive negative changes allowed the less negatively charged chaperonins to function like GroEL/ES; this increase was over and above the assistance succinate provided to spontaneous refolding (*SI Appendix*, Fig. S3*E*). Thus, the negatively charged cavity may contribute significantly toward accelerating the refolding rate of a model substrate in vitro.

Although refolding rates were not accelerated by most of the chaperonins tested at 25 °C, there could be subtle alterations in the folding landscape. This was quantitatively captured by temperature-dependent kinetic analysis using a modified Eyring and Arrhenius equation (4, 16). The temperature-dependent kinetic parameters were shown to be independent of the temperature-dependent changes in GroEL/ES allostery (16), allowing us to monitor the true nature of the sGFP folding landscape in the presence and absence of chaperonins. The temperature-dependent kinetics with cfl-EL/ES, smh-EL/ES, y-EL/ES, h-EL/ES, hHsp60/10, and yHsp60/10 (Fig. 3*E* and *SI Appendix*, Fig. S3*F*) was used to obtain the three activation parameters ΔC_p, ΔH, and ρ that define the refolding pathway (*SI Appendix*, Table S2). ΔC_p is the heat capacity change between the transition state and the refolding intermediate and is correlated to the area of solvent accessible surface area (SASA) that is lost during the process. ΔH is the change in enthalpy between the transition state and the refolding intermediate and correlates with the enthalpic trap that limits folding; a higher ΔH would indicate a larger enthalpic trap during folding. ρ denotes a complex parameter of transition frequency and entropic change between the transition state and the refolding intermediate. A higher ρ indicates an entropically favorable process, while a lower value indicates an entropically unfavorable process. The parameters were compared with reported parameters obtained from temperature-dependent kinetics of spontaneous and GroEL/ES-assisted refolding of sGFP under identical conditions (16). The most negatively charged chaperonin cfl-EL/ES was indeed more capable of increasing ρ, suggesting that the entropic component was more favorable toward folding sGFP when assisted with cfl-EL/ES. Conversely, the chaperonins with lower negative charges than GroEL/ES all show a lower ρ. A notable exception was smh-EL/ES that appears as an outlier with an entropic assistance close to that of GroEL/ES but also with a compensatory high enthalpic barrier that offsets the favorable entropic component to prevent rate acceleration by this chaperonin. The overall trend suggests that the ability of GroEL/ES to accelerate substrate folding by entropically favoring the folded state (16, 18, 19), at least partially, depends on the charge density inside the chaperonin cavity (Fig. 3*F*). Since charge density in the cavity of the chaperonins varies between organisms, entropic assistance to folding may not be a conserved feature of all the Hsp60/10 chaperonins.

Taken together, negative charge density in the cavity correlated with a chaperonin's ability to rescue entropic traps in folding pathways. It also correlated with their ability to assist in folding GroEL/ES's substrate in vivo and to replace the function of GroEL/ES in *E. coli*. Taken together, our findings suggested that the mechanism through which chaperonins assisted the folding of its substrates may have diverged along with their cavity property.

The Chaperonins Have a Conserved Ability to Regulate Hydrophobic Collapse of the Substrate. Since many of the chaperonins, either the GroEL/ES homologs or the artificially designed ones, could not function like GroEL/ES in assisting the folding of substrates, we asked if these chaperonins provide a different sort of folding assistance. From the rates of chaperonin-assisted sGFP refolding obtained at different temperatures, it was apparent that although many of them could not assist in folding entropically, the folding pathway of sGFP was significantly altered in the presence of the chaperonins. All of them except hHsp60/

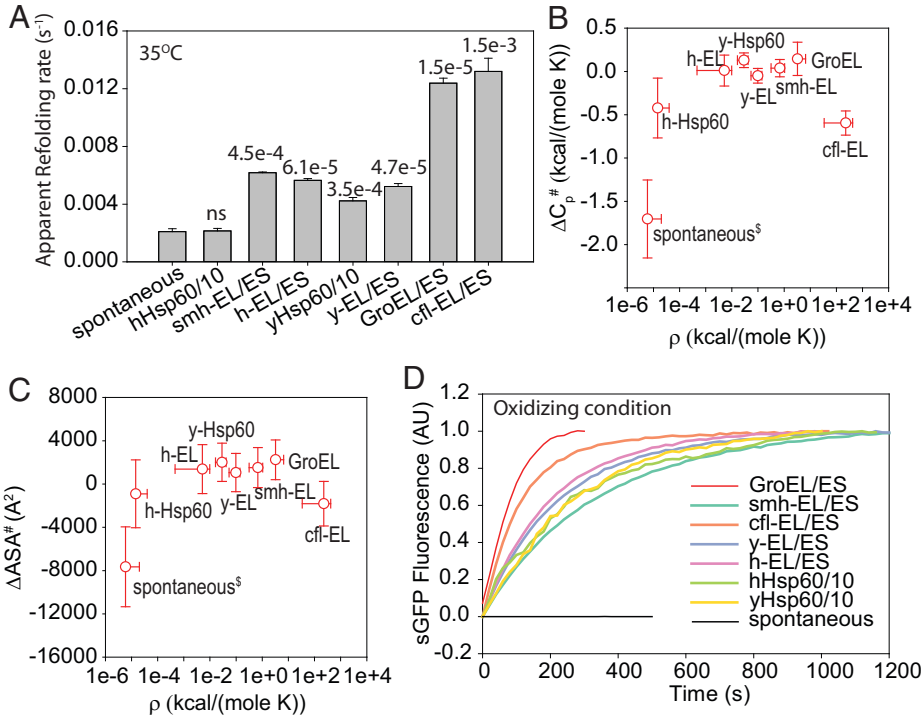

Fig. 4. Hsp60/10 chaperonins have conserved property to modify chain collapse during folding. (*A*) The apparent rate of refolding of sGFP alone or in the presence of different chaperonins (hHsp60/10, smh-EL/ES, h-EL/ES, yHsp60/10, y-EL/ES, GroEL/ES, and cfl-EL/ES, arranged in ascending order of negative charge density in the *cis*-cavity) at 35 °C. (*B* and *C*) The plots show the correlation between ΔC_p and ρ values (*B*) or between predicted $\Delta ASA^{\#}(Å^2)$ calculated from ΔC_p and ρ values (*C*) obtained from Arrhenius fitting of spontaneous or chaperonin-assisted sGFP refolding. Error bars for *B* and *C* represent the errors of fitting from nonlinear regression. $^{\$}$Parameters for spontaneous refolding are taken from published work for comparison (16). (*D*) sGFP refolding kinetics alone or in the presence of different chaperonins under oxidizing conditions. sGFP was unfolded in 6 M GuHCl for 1 h and refolded upon 100-fold dilution in buffer C.

10 assisted better with an increase in temperature and were able to accelerate the refolding of sGFP significantly at 35 °C (Fig. 4*A*), albeit not to the extent of GroEL/ES or cfl-EL/ES. This happened as spontaneous refolding became slower above 30 °C, whereas this did not dip in the presence of the chaperonins (Fig. 3*E*). This negative dip is correlated to the large negative ΔC_p associated with the spontaneous refolding pathway, whereas a relatively small ΔC_p was associated with chaperonin-assisted folding (Fig. 4*B*). ΔC_p allows us to estimate the accessible surface that is buried during the rate-limiting step of refolding (20, 21) (Fig. 4*C*), and this shows that the rate-limiting step of sGFP refolding in vitro consists of a step that buries a large surface area. The rate-limiting step of refolding in any of the chaperonins, independent of their ability to decrease the entropic trap, proceeded with little change in surface area. Importantly, monomeric GroEL was unable to alter the hydrophobic collapse efficiently; it exhibits a negative ΔC_p like spontaneous refolding (*SI Appendix*, Fig. S4*A*). Thus, efficient encapsulation inside the cavity was necessary for regulated polypeptide chain collapse. This was consistent with previous reports that folding in an enclosed cavity of chaperonin could change the rate-limiting step of folding by altering the hydrophobic collapse inside the cavity (17, 19, 22). However, while we found this to be a conserved feature of the chaperonin cages, this was not sufficient to ensure chaperonin-assisted acceleration. Thus, encapsulation in a chaperonin cavity may change the folding pathway by altering the route of hydrophobic collapse, preventing nonnative contacts; acceleration of refolding rate may be additionally supported by contributions from the charges lining the chaperonin cavity.

If hydrophobic collapse is altered by these chaperonins, they should be able to change the order of formation of contacts during folding. sGFP is known to form at least one nonnative contact during folding, namely, the interaction between C48 and C70, which are two residues that are placed distantly in the native structure (16). In the presence of oxidizing agents in the refolding buffer, this interaction is locked to irreversible block folding (Fig. 4*D*). This can be used to ask if the chaperonins prevent these residues from interacting, effectively probing if the alteration in hydrophobic collapse can prevent nonnative contacts. All the chaperones tested prevented the oxidation-dependent block in sGFP refolding (Fig. 4*D*), demonstrating that they efficiently alter the folding pathway by preventing nonnative contacts in sGFP, possibly by changing the route of hydrophobic collapse. This suggested that all the chaperonins tested were active and efficient at altering refolding pathways by regulating polypeptide chain collapse during folding. All the chaperonins tested therefore could increase the folding rate marginally at 35 °C, most likely by regulating the hydrophobic collapse, but the magnitude of rate acceleration at all temperatures was dependent on the entropic assistance by the chaperonins. Entropic assistance partly depended on the negative charge density of the *cis*-cavity; this property was not conserved between different chaperonins.

The Chaperonin Homologs Differ in Their Capacity to Buffer Mutations. Different mutations on a substrate can create different types of traps on folding pathways. If the chaperonins differ in their capability to aid different types of kinetic traps, different chaperonins should diverge in their ability to assist different mutations in a protein. This can be checked in vivo by the mutations buffered by the chaperonins. Depending on whether a mutant can take advantage of the conserved mechanism of the chaperonins or the special folding assistance of negatively charged cavity,

we should be able to identify mutants that are either buffered generally by most of the chaperonins or preferentially by the negatively charged chaperonins, like K45E, respectively.

We used a previously constructed GFP mutant library (16) that was enriched for mutations that decrease the GFP fluorescence. We could identify 5 unique clones from 10 randomly picked colonies from a plate containing ∼1,000 colonies. This demonstrated that the library contained ∼500 different mutant clones of GFP (16). High-throughput DNA sequencing of the plasmid pool could identify ∼600 mutations with high confidence (*SI Appendix*, Fig. S4*B* and Table S3), supporting the complexity.

The activity of the GFP mutant library was measured in wild-type (WT) cells in the presence or absence of the overexpressed chaperonins. Fluorescence of the mutant GFP library was internally normalized with respect to mCherry expressed as an independent protein from the same operon as GFP. mCherry fluorescence normalizes for variation in expression levels due to variability in plasmid copy number, induction, transcription, or translation. The mutant library exhibited higher GFP/mCherry fluorescence in cells overexpressing GroEL/ES and even higher in the presence of cfl-EL/ES (Fig. 5*A*). Other chaperonins failed to increase the median fluorescence of the mutant library (Fig. 5*A* and *SI Appendix*, Fig. S4*C*). Expression levels of the chaperonins differed moderately in vivo (*SI Appendix*, Fig. S4*D*) and did not follow the trend in their efficiency to assist the mutant library. To investigate if the difference in efficiency stems from expression level differences, we checked for the activity of the mutant pool of GFP at different induction levels of GroEL/ES and hHsp60/10 (*SI Appendix*, Fig. S4 *E* and *F*). The efficiency did not decrease with a ∼fourfold decrease in GroEL/ES concentrations, suggesting that there is a saturation of buffering capacity of GroEL/ES even at an ∼fourfold lower concentration (*SI Appendix*, Fig. S4 *E* and *F*); differences between the expression levels of GroEL/ES and the other chaperonins are much smaller and hence unlikely to contribute to the differences in efficiency. Additionally, the efficiency of GroEL/ES was drastically higher than hHsp60/10 at equivalent expression levels of the two chaperonins (*SI Appendix*, Fig. S4 *E* and *F*). Therefore, minor differences in expression levels did not account for the differences in chaperonin efficiencies. Thus, GroEL/ES and cfl-EL/ES were more efficient than the other chaperonins in assisting this mutant pool. This corroborated with the biophysical and genetic studies showing that these two chaperones were more potent in assisting GroEL/ES-dependent substrates and complementing GroEL/ES depletion in *E. coli*.

Since the pooled library of GFP had different mutants at different proportions, the peak fluorescence of the pool could shift even if only the most-abundant mutants are assisted by specific chaperonins without affecting a large pool of low-abundant mutants. To check the proportion of mutants assisted by the chaperonins while shifting the peak of the library, we sorted the population around the peak of the GFP/mCherry fluorescence (peak fluorescence population [PF population]) to identify mutations that were present predominantly at the median-GFP fluorescence in the presence or absence of the chaperonins (Fig. 5*B*, comparison 1). GFP variants isolated from the cells were deep sequenced to obtain relative abundance for the different mutants in the presence or absence of the chaperonins. The relative abundance of most of the ∼600 mutants identified in the PF population correlated well between cells with or without chaperonins (*SI Appendix*, Fig. S4*G*). This suggested that GroEL/ES or cfl-EL/ES shifted the median fluorescence of the mutant library by buffering most of the mutations that were present in the population. Thus, these two chaperonins can assist many mutants and the shift is, in this case, correlated to the negative charge density inside the cavity.

On similar lines as above, it is also possible that the other chaperonins affect a different subset of low-abundant mutants and hence do not shift the median of the pooled library. To check this, we sorted out the top 5 to 10% of the fluorescent cells (highly fluorescent [HF] population) in the presence and absence of the chaperonins (Fig. 5*B*). Normalization of the reads in HF with PF provided an enrichment score (Esc) for each mutant in the presence of each of the different chaperonins. In the absence of any assistance (or obstruction) by a chaperonin, mutants would be similarly enriched (or depleted) in the HF region in the presence or absence of the chaperonin. The log-transformed ratio of Esc in the presence versus absence of a chaperonin overexpression provided a quantitative measure of assistance. We termed this the buffering index (BI), which was measured for each mutant in the presence of each of the chaperonins. A mutant that is unaffected by chaperonin would have a BI close to zero, an assisted mutant would have it more than zero, and a disfavored substrate would have a negative BI. This index enabled us to detect the hidden assistance of low-abundant GFP mutants by the different chaperonins. The BI of each chaperone for ∼600 mutants provides the spectrum of mutations that each chaperone preferentially buffers (Fig. 5*C*). Clustering the chaperones based on their BI for the different mutants segregated GroEL/ES and cfl-EL/ES from the others (Fig. 5*C*). Thus, these two chaperonins prefer to assist a distinct set of mutants and hence may be mechanistically different from the other chaperones tested.

By clustering the mutants, we were able to identify mutants that were specifically buffered by GroEL and cfl-EL/ES and not by the other chaperones (Fig. 5*D*, cluster 1) or were specific for yHsp60 (Cluster 4) or yHsp60 and hHsp60 (Fig. 5*D*, cluster 3). A group of mutants was found to be buffered by all the chaperones (Fig. 5*D*, cluster 2). From cluster 2, we reconstituted the V12L mutant and confirmed that this mutant was indeed assisted by all the tested chaperonins in vivo (Fig. 5*E*). The chimeric chaperonins could also assist it to fold in vivo (*SI Appendix*, Fig. S4*H*), while a general holdase DnaK/J/E did not help it fold in vivo (*SI Appendix*, Fig. S4*I*). Thus, this mutant is indeed dependent specifically upon the chaperonins for folding in vivo and not on the general holdase function of chaperones. Interestingly, hHsp60/10 or yHsp60/10 systems were marginally more efficient in chaperoning this mutant than GroEL/ES (Fig. 5*E*). The presence of this cluster corroborates our mechanistic finding that there is a conserved mechanism of substrate assistance among all these chaperonins (as seen for cluster 2 mutants) and special divergent mechanisms that are seen as a difference between the chaperones in the other clusters of mutants.

The specific mutations of cluster 1 or cluster 3 were mapped on the structure of GFP (Fig. 5*F*). Mutants of both the clusters are completely or partially buried (Fig. 5*G*). Additionally, mutants in both clusters were predicted to be highly destabilizing and were involved in forming intramolecular contacts (Fig. 5*H*). This suggests that while being different in their specificity, both the groups of chaperonins can assist mutants with a potentially altered stability or folding pathway.

Since the cfl-EL/ES and GroEL/ES chaperonins have higher negative charge potential inside the cavity, we asked if there were differences among the chaperonins in their preferences for mutations on charged residues. We found that cfl-EL/ES or

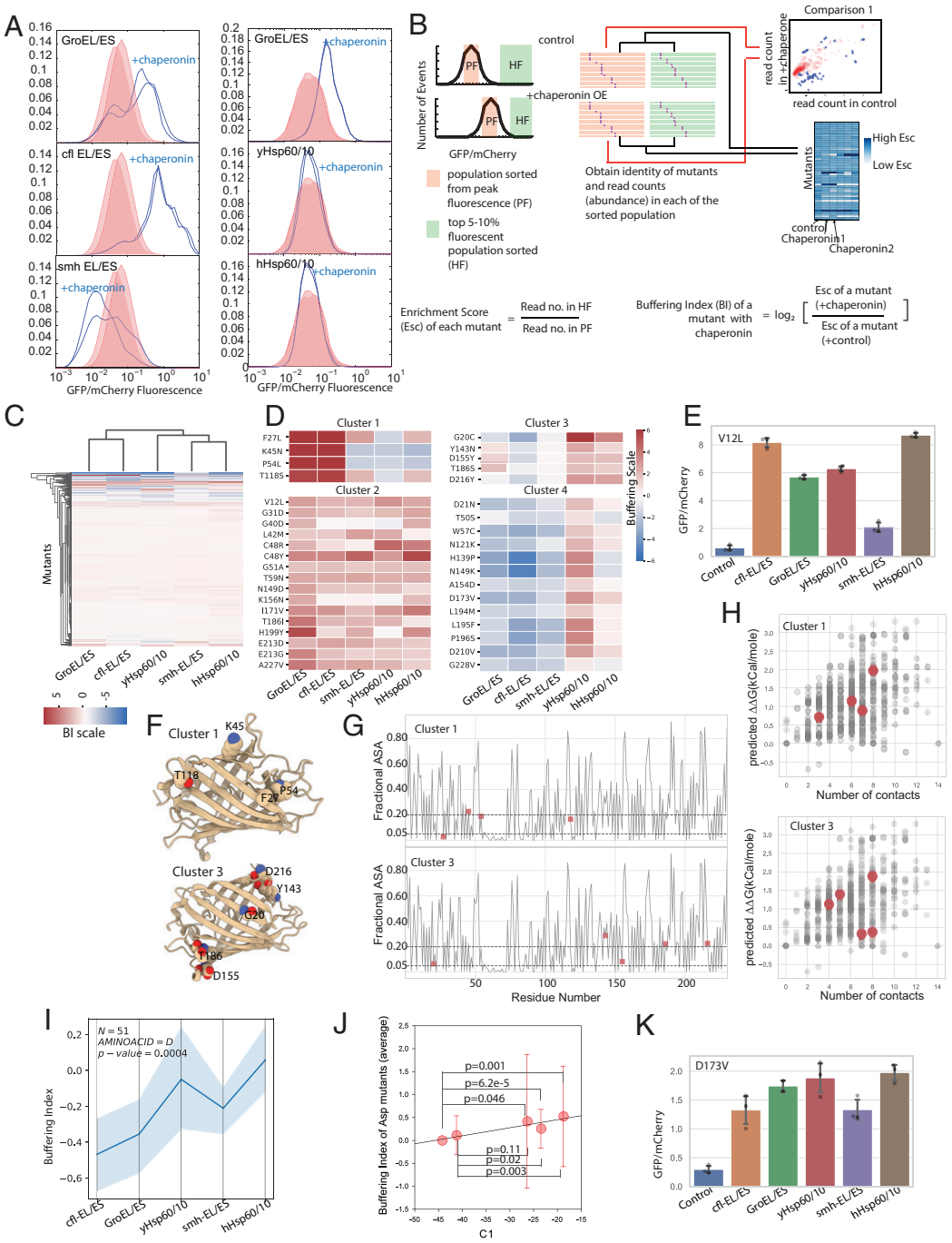

Fig. 5. Chaperonin homologs have a divergent spectrum of mutants buffered. (*A*) Histogram of GFP/mCherry fluorescence of the pooled mutant library of GFP in the absence and presence of different chaperones. Red-shaded areas show the distribution of fluorescence in the absence of chaperones and the same data are shown in each group of vertical panels to show the effect of chaperonins. Biological duplicates are shown in the figure. (*B*) Schematic for identifying the mutations that are assisted by each of the chaperonins. Highly fluorescent clones (top ~5%, HF) and the median fluorescent clones (around peak, PF) were isolated from either control cells not overexpressing chaperonins or from cells overexpressing a test chaperonin system (GroEL/ES, cfl-EL/ES, smh-EL/ES, hHsp60/10, yHsp60/10). Mutants in these populations were identified and quantified using next-generation sequencing (NGS) and processed to obtain the correlation in read counts between control and chaperonin-overexpressing cells in the HF population. Escs were calculated for each mutant by dividing the read counts obtained for the mutant in HF by the read counts in PF. The BI of each mutant in the presence of each of the chaperonins was calculated by taking the log of the ratio of the Esc of the mutant in presence and absence of a particular chaperonin. (*C*) BI of the mutants were used to cluster the chaperonins. This clustered the chaperonins based on the similarity of the spectrum of mutations buffered by each of them. (*D*) Heatmap to show the activity of mutants, from representative clusters from *C*, in the presence of different chaperonins. All mutants show a *P* value of <0.05 in the presence of at least one of the chaperonins based on the Wilcoxon test. (*E*) Quantitation of GFP/mCherry fluorescence of GFP (V12L) mutant in the presence and absence of the different chaperonins. Three biological replicates for each experiment were averaged, and the error bars are SDs. (*F*) Mutations present in cluster 1 and cluster 3 in *C* mapped in the crystal structure of GFP (1GFL) (36). (*G*) Accessibility of the residues mutated in cluster 1 and 3 from *C*. ASA, accessible surface area. (*H*) Predicted ΔΔG of the different mutants (predicted from the structure using PremPS) (37), plotted against the number of contacts formed by each of the residues. In gray are all the mutants identified in NGS, and red are the mutants in cluster 1 or 3 from *C*. (*I*) The median BI of mutants that has an endogenous Asp substituted by other residues, in the presence of different chaperonins. In blue shade is shown the 99% confidence interval. The *P* value shown is calculated using ANOVA. Each set has BI for 51 mutants with two biological replicates. (*J*) Correlation of the mutants from *I* with the electrostatic potential at the center of the chaperonins cavity (C1). The bars shown are SDs from the data. (*K*) Quantitation of GFP/mCherry fluorescence of GFP (D173V) mutant in the presence and absence of the different chaperonins. Three biological replicates were done for each experiment.

GroEL/ES disfavored mutants where an endogenous Asp (D) was mutated to other residues, which the other chaperones did not (Fig. 5*I*). Importantly, the chaperonins showed a linear trend in the buffering capacity of these mutants with the negative charge density of the cavity (Fig. 5*J*). This was confirmed by isolating the mutant GFP(D173V), from the pool (Fig. 5*K*). This mutant indeed showed the trend observed for Asp mutants in the pool that the buffering capacity is higher in the less negatively charged chaperonins than in the more negatively charged ones. Other charged residues did not show any significant difference between the different chaperonins (*SI Appendix*, Fig. S4*J*). This suggested that the negatively charged cage may support the folding of negatively charged substrates more efficiently, as suggested earlier (12, 13, 23).

Taken together, the buffering capacity of cfl-EL/ES seems to be the highest, followed by GroEL/ES as they shift the peak fluorescence of the complete mutant pool. However, a more sensitive sequencing-based assay delineates the similarities and differences in the buffering spectrum for each of the chaperonins. This highlights similarities in a core mechanism and differences in specialized mechanisms among the two clusters. This corroborates well with our biochemical findings on the activity of the different chaperones; they have a conserved mode of action on substrates and a specialized mode that diverges between the different chaperonins.

Discussion

Chaperonins have evolved to cater to specific problems faced by organisms in their niches. This depends on the environment as well as the protein sequences that diverge between species. Here, we show that GroEL/ES caters to its proteome efficiently by two mechanisms, namely, regulated chain collapse and entropic assistance to folding. While the former is conserved between the different Hsp60/10 chaperonins tested, the latter has diverged and is partially dependent on the negative charge density in the folding cavity of GroEL/ES.

Since we have focused specifically on the negative charge property of the cavity in this report, there are certain limitations. First, the chimeric constructs are derived from extensive insertions, albeit, from homologous regions of two chaperonins. They retain their biochemical functionality in all the assays performed but may have cryptic changes in allostery that contribute partly to the differences. However, our supplementation experiments with negatively charged small molecules imply that a large part of the difference in the chaperoning mechanism is contributed by the negatively charged surface. Second, we need to carefully understand the link between cavity charges, detailed structural features, allosteric properties, and the chaperoning capacity of the different GroEL/ES homologs. Finally, the presence of mutants that are efficiently buffered by the less negatively charged chaperonins calls our attention toward specialized mechanisms that we have not yet understood.

GroEL/ES and other chaperones have been shown to alter the folding energy landscape by reducing ruggedness (24–26). Barrel-shaped chaperonins can be classified as class I (found in prokaryotes, organelles of endosymbiotic origin in eukaryotes, and some archaea, and works with the cochaperone Hsp10 that acts as a lid) or class II (found in eukaryotic cytosol and archaea and does not require another protein to act as a lid) chaperonins. Both of these classes of chaperonins may change the entropic barriers to refolding (16, 18, 27) through the negative charges inside the cavity (22) or confinement in the enclosed cis-cavity (12, 13). It may also unfold proteins (17, 28), regulate the hydrophobic collapse (17, 19, 22), and prevent the formation of nonnative contacts during folding (16). Within the limitations of the current study, we tested if the different chaperonins changed the folding landscape of sGFP by changing the energetics of the rate-limiting step. While the rate-limiting step of spontaneous refolding of the model substrate in solution was dominated by a large surface area being buried in the transition state of folding, chaperonin-assisted folding was routed through a pathway with minimal surface burial. This suggests that all the chaperonins tested shared a conserved feature to alter the folding landscape by altering the way unfolded polypeptide chains collapse. This is coherent with a previous report that GroEL/ES releases the substrate in a regulated manner (17, 19) and prevents the cooperative collapse of DapA (19). Therefore, GroEL/ES prevents a step that would bury a large surface area; all of the chaperonins tested were able to regulate the release of sGFP similarly, indicating this to be a conserved process. Hsp60 chaperonins undergo a large conformational change upon ATP and Hsp10 binding to release the substrate inside the *cis*-cavity. This change is accompanied by a decrease in surface hydrophobicity of the cavity; the regulated collapse of the unfolded substrate may be controlled by this release mechanism that is conserved among the chaperonins.

A closer look at the folding landscape reveals that enthalpic barriers do not decrease during chaperonin-dependent folding of sGFP. The entropic barriers decrease as a function of the negative charge density inside the *cis*-cavity of the chaperonin. The importance of conserved negative charges is known in this context (13, 18) and may indeed proceed through repulsion between the negatively charged surface of the folded substrate and the cavity wall (12, 29), making it a nonstick surface while repelling the negatively charged residue to aid the resolution of entropic traps. Consistent with this, we found that mutant proteins that harbor mutations that remove negative charges (Asp) from the surface of GFP are less likely to be substrates of the negatively charged chaperones than of the less negatively charged ones (Fig. 5 *I* and *J*).

While negative charge density is only one aspect of GroEL's structure that aids folding, there may be other aspects that contribute to GroEL's ability to accelerate folding (30). It is also possible that the eukaryotic or the less negatively charged prokaryotic homologs work in concert with small molecules, like the negatively charged small molecule succinate, to exert their full chaperoning potential in vivo. We see a clear case of synergism between the eukaryotic Hsp60/10 chaperonins and succinate that may hint toward an environment-specific activity that would need to be explored to fully appreciate the function of these chaperonins in their native setting. Additionally, the charge distribution on substrates may differ between organisms depending on the average isoelectric point (pI) of their proteome. Thus, it is likely that these chaperonins may have evolved specific properties that accommodate their native substrates in their native cellular milieu.

Notably, eukaryotic Hsp60/10s have significantly high numbers of hydroxyl groups pointing inside the cavity. Given the potential of polyols to act as chemical chaperones, we posit that each of these chaperonins have evolved a unique mechanism to assist folding, dependent on the nature of their substrates. It is possible that the complexity of the domains and domain organization in chaperonin substrates also play an important role in selecting the most appropriate mechanisms of folding assistance by chaperonins. It is therefore likely, as we find in the case of mutational buffering, that these chaperones would accelerate the folding of their substrates but with different mechanisms,

just as different chemical chaperones use different mechanisms to accelerate folding (4). Further work in this area would be required to test this possibility.

While the chaperonins tested show differences in activities, their divergence, given the possibilities above, would be best tested with their endogenous substrates in their native settings. While in vitro work points toward mechanistic differences between these chaperonins and their difference in affecting mutational buffering, further work in vivo will be required to fully appreciate this remarkable difference between these chaperones and their collaboration with their chemical milieu.

Materials and Methods

Experimental Model and Subject Details.

Strains, plasmids, and proteins. *E. coli* strain DH5α was used for cloning, WT *E. coli* K-12 (BW25113) strain was used for the expression of arabinose-inducible pBAD GFP, and BL21 (DE3) was used for protein expression and purification. Deletion strains were obtained from *E. coli* Genetic Stock Center (CGSC) as part of the Keio collection (31). Further details are provided in the *SI Appendix, Supplemental Methods*.

Modeling and identification of inner-lining residues of Hsp60/10 cavities. Modeling was performed using Modeler v9.17 (32) with the crystal structure of asymmetric chaperonin complex of GROEL/ES as the template (PDB: 1AON) (33). We identified inner-lining constituent amino acids of Hsp60/10 cavities by using CICLOP (8). Further details are provided in *SI Appendix, Supplemental Methods*.

Spontaneous and chaperonin-assisted in vitro refolding of sGFP. Refolding and solubility and ATPase assays were performed as previously reported (16, 34). Temperature-dependent refolding was done as described earlier (16). Further details are provided in *SI Appendix, Supplemental Methods*.

GFP-mutant buffering in pooled library. GFP mutant libraries were transformed in WtK cells that harbored the different chaperonin-expressing constructs. Sorting was performed using fluorescence-assisted cell sorting, and the mutants were identified and quantified using high-throughput sequencing. Further details are provided in *SI Appendix, methods*.

Quantification and Statistical Analysis. Student *t* test and R package for nonlinear regression were used for statistical analysis. Flow-cytometry data were analyzed using MATLAB using in-house scripts.

Data Availability. All study data are included in the article and/or *SI Appendix*.

ACKNOWLEDGMENTS. We thank Prof. Hideki Taguchi for the kind gift of MGM100 strain and pET21 SR1 plasmid. We thank Kanika Saxena for sharing the starting plasmid with GFP and mCherry. K.M. acknowledges funding from the Department of Biotechnology (DBT), Government of India (Grant number BT/PR28386/BRB/10/1671/2018) and Science and Engineering Research Board (SERB), Government of India, for Core Research Grant (SERB/CRG/2019/006281) and Shiv Nadar University (SNU) core funding. K.C. acknowledges grant support from DST (DST/SJF/LSA-01/2015-16) and partly by BSC0124 from Council of Scientific and Industrial Research (CSIR). Instrument support was also obtained from Wellcome Trust–DBT India Alliance and CSIR. K.C. is a DBT–Wellcome Trust India Alliance Senior Fellow. K.M. and M.A. acknowledge SNU for infrastructural support, and K.C. acknowledges CSIR and CSIR–Institute of Genomics and Integrative Biology for infrastructural support. A. Sadat, S.T., and A.C. acknowledge DBT; Z.Z., K.B.N.R., M.T., and K.V., acknowledge CSIR. M.K., A. Sharma, A.G., and D.G. acknowledge University Grants Commission for fellowship support. M.A. acknowledges SNU doctoral fellowship.

Author affiliations: [a]Academy of Scientific and Innovative Research (AcSIR), Ghaziabad 201002, India; [b]Chemical and System Biology Unit, CSIR–Institute of Genomics and Integrative Biology, New Delhi 110025, India; [c]Department of Computational Biology, Indraprastha Institute of Information Technology–Delhi, New Delhi 110020, India; and [d]Department of Life Sciences, School of Natural Sciences, Shiv Nadar University, Greater Noida 201314, India

1. M. Hayer-Hartl, A. Bracher, F. U. Hartl, The GroEL-GroES chaperonin machine: A nano-cage for protein folding. *Trends Biochem. Sci.* **41**, 62–76 (2016).
2. A. L. Horwich, G. W. Farr, W. A. Fenton, GroEL-GroES-mediated protein folding. *Chem. Rev.* **106**, 1917–1930 (2006).
3. L. Cortez, V. Sim, The therapeutic potential of chemical chaperones in protein folding diseases. *Prion* **8**, 197–202 (2014).
4. R. Dandage *et al.*, Classification of chemical chaperones based on their effect on protein folding landscapes. *ACS Chem. Biol.* **10**, 813–820 (2015).
5. A. Bandyopadhyay *et al.*, Chemical chaperones assist intracellular folding to buffer mutational variations. *Nat. Chem. Biol.* **8**, 238–245 (2012).
6. K. Verma *et al.*, Distinct metabolic states of a cell guide alternate fates of mutational buffering through altered proteostasis. *Nat. Commun.* **11**, 2926 (2020).
7. M. J. Kerner *et al.*, Proteome-wide analysis of chaperonin-dependent protein folding in Escherichia coli. *Cell* **122**, 209–220 (2005).
8. P. Garg *et al.*, CICLOP: A robust and accurate computational framework for protein inner cavity detection. *Bioinformatics*, 10.1093/bioinformatics/btac061 (2022).
9. D. Chrétien *et al.*, Mitochondria are physiologically maintained at close to 50 °C. *PLoS Biol.* **16**, e2003992 (2018).
10. A. Ojha *et al.*, GroEL1: A dedicated chaperone involved in mycolic acid biosynthesis during biofilm formation in mycobacteria. *Cell* **123**, 861–873 (2005).
11. Y. Zhang, J. Skolnick, Scoring function for automated assessment of protein structure template quality. *Proteins* **57**, 702–710 (2004).
12. Y. C. Tang, H. C. Chang, K. Chakraborty, F. U. Hartl, M. Hayer-Hartl, Essential role of the chaperonin folding compartment in vivo. *EMBO J.* **27**, 1458–1468 (2008).
13. Y. C. Tang *et al.*, Structural features of the GroEL-GroES nano-cage required for rapid folding of encapsulated protein. *Cell* **125**, 903–914 (2006).
14. S. Nisemblat, A. Parnas, O. Yaniv, A. Azem, F. Frolow, Crystallization and structure determination of a symmetrical "football" complex of the mammalian mitochondrial Hsp60-Hsp10 chaperonins. *Acta Crystallogr. F Struct. Biol. Commun.* **70**, 116–119 (2014).
15. P. V. Viitanen *et al.*, Mammalian mitochondrial chaperonin 60 functions as a single toroidal ring. *J. Biol. Chem.* **267**, 695–698 (1992).
16. A. Sadat *et al.*, GROEL/ES buffers entropic traps in folding pathway during evolution of a model substrate. *J. Mol. Biol.* **432**, 5649–5664 (2020).
17. S. Sharma *et al.*, Monitoring protein conformation along the pathway of chaperonin-assisted folding. *Cell* **133**, 142–153 (2008).
18. K. Chakraborty *et al.*, Chaperonin-catalyzed rescue of kinetically trapped states in protein folding. *Cell* **142**, 112–122 (2010).
19. F. Georgescauld *et al.*, GroEL/ES chaperonin modulates the mechanism and accelerates the rate of TIM-barrel domain folding. *Cell* **157**, 922–934 (2014).
20. J. R. Livingstone, R. S. Spolar, M. T. Record Jr., Contribution to the thermodynamics of protein folding from the reduction in water-accessible nonpolar surface area. *Biochemistry* **30**, 4237–4244 (1991).
21. J. K. Myers, C. N. Pace, J. M. Scholtz, Denaturant m values and heat capacity changes: Relation to changes in accessible surface areas of protein unfolding. *Protein Sci.* **4**, 2138–2148 (1995).
22. A. K. Singh, D. Balchin, R. Imamoglu, M. Hayer-Hartl, F. U. Hartl, Efficient catalysis of protein folding by GroEL/ES of the obligate chaperonin substrate MetF. *J. Mol. Biol.* **432**, 2304–2318 (2020).
23. A. J. Gupta, S. Haldar, G. Miličić, F. U. Hartl, M. Hayer-Hartl, Active cage mechanism of chaperonin-assisted protein folding demonstrated at single-molecule level. *J. Mol. Biol.* **426**, 2739–2754 (2014).
24. R. Imamoglu, D. Balchin, M. Hayer-Hartl, F. U. Hartl, Bacterial Hsp70 resolves misfolded states and accelerates productive folding of a multi-domain protein. *Nat. Commun.* **11**, 365 (2020).
25. D. Balchin, M. Hayer-Hartl, F. U. Hartl, Recent advances in understanding catalysis of protein folding by molecular chaperones. *FEBS Lett.* **594**, 2770–2781 (2020).
26. J. Lu *et al.*, Energy landscape remodeling mechanism of Hsp70-chaperone-accelerated protein folding. *Biophys. J.* **120**, 1971–1983 (2021).
27. D. Balchin, G. Milicic, M. Strauss, M. Hayer-Hartl, F. U. Hartl, Pathway of actin folding directed by the eukaryotic chaperonin TRiC. *Cell* **174**, 1507–1521.e1516 (2018).
28. D. S. Libich, V. Tugarinov, G. M. Clore, Intrinsic unfoldase/foldase activity of the chaperonin GroEL directly demonstrated using multinuclear relaxation-based NMR. *Proc. Natl. Acad. Sci. U.S.A.* **112**, 8817–8823 (2015).
29. J. L. England, D. Lucent, V. S. Pande, A role for confined water in chaperonin function. *J. Am. Chem. Soc.* **130**, 11838–11839 (2008).
30. J. D. Wang, C. Herman, K. A. Tipton, C. A. Gross, J. S. Weissman, Directed evolution of substrate-optimized GroEL/S chaperonins. *Cell* **111**, 1027–1039 (2002).
31. T. Baba *et al.*, Construction of *Escherichia coli* K-12 in-frame, single-gene knockout mutants: The Keio collection. *Mol. Syst. Biol.* **2**, 2006.0008 (2006).
32. N. Eswar *et al.*, Comparative protein structure modeling using Modeller. *Curr. Protoc. Bioinformatics* **Chapter 5**:Unit-5.6 (2006).
33. Z. Xu, A. L. Horwich, P. B. Sigler, The crystal structure of the asymmetric GroEL-GroES-(ADP)7 chaperonin complex. *Nature* **388**, 741–750 (1997).
34. O. Yifrach, A. Horovitz, Nested cooperativity in the ATPase activity of the oligomeric chaperonin GroEL. *Biochemistry* **34**, 5303–5308 (1995).
35. N. A. Baker, D. Sept, S. Joseph, M. J. Holst, J. A. McCammon, Electrostatics of nanosystems: Application to microtubules and the ribosome. *Proc. Natl. Acad. Sci. U.S.A.* **98**, 10037–10041 (2001).
36. F. Yang, L. G. Moss, G. N. Phillips Jr., The molecular structure of green fluorescent protein. *Nat. Biotechnol.* **14**, 1246–1251 (1996).
37. Y. Chen *et al.*, PremPS: Predicting the impact of missense mutations on protein stability. *PLOS Comput. Biol.* **16**, e1008543 (2020).